# Olefin Oligomerization by Main Group $Ga^{3+}$ and $Zn^{2+}$ Single Site Catalysts

**Nicole LiBretto**
National Renewable Energy Lab https://orcid.org/0000-0002-6922-2790
**Yinan Xu**
Purdue University West Lafayette
**Aubrey Quigley**
Purdue University West Lafayette
**Ethan Edwards**
Purdue University West Lafayette https://orcid.org/0000-0002-0973-193X
**Rhea Nargund**
Purdue University West Lafayette
**Juan Vega-Vila**
Purdue University West Lafayette
**Arunima Saxena**
Purdue University West Lafayette
**Rajamani Gounder**
Purdue University West Lafayette https://orcid.org/0000-0003-1347-534X
**Jeffrey Greeley**
Purdue University
**Guanghui Zhang**
Dalian University of Technology https://orcid.org/0000-0002-5854-6909
**Jeffrey Miller** ( mill1194@purdue.edu )
Purdue University West Lafayette https://orcid.org/0000-0002-6269-0620

---

**Article**

**Keywords:** Silica-supported Catalysts, Cossee-Arlman Mechanism, Metal Hydride and Metal Alkyl Intermediates, Olefin Processes

**Posted Date:** October 23rd, 2020

**DOI:** https://doi.org/10.21203/rs.3.rs-94946/v1

**Version of Record:** A version of this preprint was published at Nature Communications on April 19th, 2021. See the published version at https://doi.org/10.1038/s41467-021-22512-6.

# Abstract

In heterogeneous catalysis, olefin oligomerization is typically performed on immobilized transition metal ions, such as $Ni^{2+}$ and $Cr^{3+}$. Here we report that silica-supported, single site catalysts containing immobilized, main group $Zn^{2+}$ and $Ga^{3+}$ ions catalyze ethylene and propylene oligomerization to an equilibrium distribution of linear olefins with rates similar to that of $Ni^{2+}$. The molecular weight distribution of products formed on $Zn^{2+}$ is similar to $Ni^{2+}$; while $Ga^{3+}$ forms higher molecular weight olefins. *In situ* spectroscopic and computational studies suggest that oligomerization unexpectedly occurs by the Cossee-Arlman mechanism via metal hydride and metal alkyl intermediates formed during olefin insertion and β-hydride elimination elementary steps. Initiation of the catalytic cycle is proposed to occur by heterolytic C-H dissociation of ethylene, which occurs at about 250°C where oligomerization is catalytically relevant. This work reports new chemistry for main group metal catalysts with potential for development of new olefin processes.


# Introduction

Olefin oligomerization to produce higher molecular weight olefins was commercialized in the 1960's and often utilizes homogeneous, transition metal catalysts containing $Cr^{3+}$ and $Ni^{2+}$.[1–3] Commercial processes utilizing Ni-based homogeneous catalysts include Shell Higher Olefins and Paraffins (SHOP), SABIC/Linde alpha-SABLIN, DuPont's Versipol™, IFP AlphaSelect™, UOP Linear-1™ Chevron Philips (Gulf) and others.[1,4,5,6] Such homogeneous catalysts often require aluminum-alkyl co-catalysts to form the initial metal-alkyl reaction intermediate. In order to obtain a high selectivity for linear α-olefins, mild reaction temperatures ranging from 30 °C-170 °C are generally used.[7–9] High pressures, often greater than 25 atm, are required to obtain high olefin conversion.[10] Homogeneous $Ni^{2+}$ catalysts offer high oligomerization rates, and the selectivity is often tailored to favor low molecular weight, linear α-olefins, useful for polymer applications.[4,10,11] Separation and regeneration of homogenous catalysts is generally not possible; thus, there is interest in development of heterogeneous catalysts, which are readily separated from the products and can be regenerated. The latter include immobilized $Ni^{2+}$ sites on zeolite (BEA, MFI), or mesoporous aluminosilicates (MCM-41) and other high surface area oxide supports, which also contain Brønsted acid sites, for example, bifunctional catalsts.[10,12–17] Supported, heterogeneous oligomerization catalysts typically do not require an aluminum alkyl co-catalyst and have lower activity, generally requiring higher operating temperatures than homogeneous catalysts.

For homogeneous and heterogeneous Ni-based catalysts, the Cossee-Arlman reaction mechanism (Scheme 1) is generally accepted. Ni-alkyl and hydrides are proposed key reaction intermediates, and olefin insertion and β-hydride elimination are the key elementary reaction steps, though limited spectroscopic evidence exists.[18,19] Activation and initiation of the catalytic cycle often occurs by alkyl transfer from an Al-alkyl co-catalyst to the Ni complex. Chain growth occurs by olefin insertion. β-hydride elimination of the longer metal alkyl leads to the olefin products and the formation of a metal hydride intermediate. Ethylene insertion to the metal hydride regenerates the metal alkyl intermediate completing

the catalytic cycle.[12,13] It is generally accepted that empty d orbitals of the transition metal catalysts are required for olefin coordination-insertion and β-hydride elimination and the formation of metal alkyl and metal hydride reaction intermediates.[20]

Recently, silica-supported, single site $Ga^{3+}$ and $Zn^{2+}$ were reported for alkane dehydrogenation and olefin hydrogenation where metal hydride and alkyl intermediates and olefin insertion and β-hydride elimination elementary steps were proposed.[22–26] Based on the common reaction intermediates and elementary steps, we hypothesize that there is a mechanistic relationship between dehydrogenation, hydrogenation and oligomerization reaction pathways and show that single site $Ga^{3+}$ and $Zn^{2+}$ also catalyze olefin oligomerization, albeit under different reaction conditions than the former reactions. The spectroscopic and theoretical evidence demonstrate the formation of reaction intermediates and elementary steps characteristic transition metal Cossee-Arlman oligomerization mechanism also occurs on these main group metal ions.

# Results

# Initial Catalyst Structure

The initial, or pre-catalyst, structure was determined by *in situ* X-ray absorption spectroscopy (XAS), including both XANES and EXAFS (Table S1) on $Ga/SiO_2$ and $Zn/SiO_2$ and compared to that of $Ni/SiO_2$. The catalysts were dehydrated at 550 °C in He and compared to known reference compounds at each metal edge (Figure S1). $Ga/SiO_2$ and $Zn/SiO_2$ have a similar structure to $Ni/SiO_2$, in that each has 4 M-O bonds with no evidence of M-O-M higher shell scattering (M = Ni, Ga, Zn). The M-O bond distances for Ga, Zn and Ni are 1.81, 1.98 and 2.03 Å, respectively (Table S1). These results are consistent with previous single site structures reported for $Ga^{3+}$, $Zn^{2+}$ and $Ni^{2+}$ hydrogenation and dehydrogenation catalysts.[23,24,27,28] These structures differ from organometallic catalysts where metal alkyls, like trimethylgallium, were grafted to a $SiO_2$ support resulting in M-M bonds.[29–31] The rates and selectivities of single site $Ga/SiO_2$ and $Zn/SiO_2$ for propylene hydrogenation and propane dehydrogenation are similar to those previously reported (Table S2,S3).[24,32] Taken together, the XAS structures and catalytic performance confirm that single site, main group $Zn^{2+}$ and $Ga^{3+}$ silica supported catalysts have been prepared in agreement to previous literature.

# Olefin Oligomerization

At 1 atm and varying $C_2H_4$ space velocities, up to 5% conversion was obtained at 250 °C with stable performance for at least 40 hours for both $Ga/SiO_2$ and $Zn/SiO_2$. The reaction rate was calculated by normalizing the rate of butene formation by the total moles of metal and increased in the order of $Ni^{2+}$ > $Ga^{3+}$ > $Zn^{2+}$ (Fig. 1a, Table S4). $Ni^{2+}$ is known for its high selectivity to dimers (*i.e.* butenes). On $Ni/SiO_2$, at 5% conversion, there is a high selectivity towards butenes ($C_4^=$, 86%) with lower selectivity towards

hexenes ($C_6^=$, 12%). Trace octenes ($C_8^=$) and higher molecular weight products are formed, along with a small amount of ethane ($C_2H_6$, < 2%).

For $Ga/SiO_2$ at the same conversion (5%), the $C_4^=$ selectivity (76%) is lower and the $C_6^=$ (17%) and $C_8^=$ (6%) selectivities are higher than those observed for $Ni/SiO_2$. $Ga/SiO_2$ has a comparable reaction rate to $Ni/SiO_2$. Single site $Zn/SiO_2$ also has a similar selectivity to $C_4^=$ (86%) as $Ni/SiO_2$.[12] The reaction rate (per metal) of $Zn/SiO_2$, however, is three times lower than that of $Ni/SiO_2$ and $Ga/SiO_2$. The $C_2H_6$ selectivity of $Zn/SiO_2$ is also higher (~ 12%) than on $Ni/SiO_2$ and $Ga/SiO_2$. At low conversion, oligomerization leads to formation of $C_4^=$ with an equilibrium distribution of 1-butene, cis-2-butene, and trans-2-butene. No isobutene ($iC_4^=$) was observed on any of these catalysts, indicating that there is no skeletal isomerization and only olefin isomerization occurs. Higher molecular weight products were also an equilibrium distribution of linear olefins.

Higher $C_2H_4$ conversion can be achieved at higher reaction pressures. In addition, higher molecular weight olefins are also formed (Fig. 1b). For example, at 250 °C and 30.6 atm $C_2H_4$, conversions up to 20%, and rates two orders of magnitude higher than those at atmospheric pressures, were obtained (Fig. 1b, Table S5). The results in Table S5 include only the quantification of gas-phase products, where a 70–80% carbon balance was achieved. At higher rates, the selectivity toward ethane on all catalysts decreased to < 0.5%, as higher conversion of $C_2H_4$ favored oligomerization over hydrogenation (Table S5). Liquid products were collected continuously during the reaction and were analyzed by mass spectrometry (GC-MS) for determination of the higher molecular weight products. On $Ga/SiO_2$, the liquid phase products include olefin hydrocarbons up to $C_{18}$. In addition, there were small amounts of paraffins and saturated rings, but there was little evidence of branched olefins. This distribution is consistent with the non-acidic nature of the inert $SiO_2$ support. $SiO_2$ does not facilitate catalytic transformations under these reaction conditions.

The product distributions on each catalyst can be described by a Schulz Flory distribution, which is determined by the ratio of the rate of olefin insertion, or propagation (α), to β-hydride elimination, or termination (1-α), and can be determined from the slope of the ln(product yield) verses carbon number.[33] The molecular weight distribution for these catalysts for $C_2H_4$ oligomerization are shown in Fig. 1c. The Schultz Flory coefficient for $C_2H_4$ oligomerization for $Ga/SiO_2$ ($\alpha_{Ga}$) is 0.59, while that of $Zn/SiO_2$ ($\alpha_{Zn}$) is 0.18, and $Ni/SiO_2$ ($\alpha_{Ni}$) is 0.22. $Ni^{2+}$ is known for olefin dimerization and reported α values are between 0.2–0.3.[12,34] $Zn^{2+}$, like $Ni^{2+}$, favors low molecular weight products like butenes, while $Ga^{3+}$ produces some higher molecular weight oligomers at the same conversion.

For comparison, $C_3H_6$ oligomerization was also performed at 1 atm and 250 °C with product selectivities and rates given in Table S6. The propylene oligomerization rate is 2–4 times higher than that for ethylene, and the Schulz Flory coefficient (Fig. 1d) was slightly higher, for example, $Ga/SiO_2$ ($\alpha_{Ga}$ = 0.70) and

$Zn/SiO_2$ ($\alpha_{Zn}$ = 0.40), which is consistent with the Schultz Flory trends observed for propylene compared to ethylene for other transition metal oligomerization catalysts.[35]

# Evidence for Oligomerization Intermediates on $Ga/SiO_2$ and $Zn/SiO_2$

$Ga^{3+}$ and $Zn^{2+}$ catalysts have been proposed to heterolytically dissociate $H_2$ and C-H bonds, for example, during olefin hydrogenation and alkane dehydrogenation, respectively. Heterolytic dissociation of $H_2$ on $Ga^{3+}$ and $Zn^{2+}$, or other single site catalysts, forms a M-H bond, *i.e.*, a hydride ($H^-$), and a proton ($H^+$), which coordinates to the M-O-Si support bond.[22,36,37] Protonation of the bridging O atom leads to breaking of the M-O bond and formation of a new Si-OH group.[24,27,32] *In situ* spectroscopic studies for these reactions and intermediates, however, have generally been obtained on catalysts at much higher temperatures (> 500°C) than those for olefin oligomerization, *ca.* 250°C. Here, we provide experimental evidence for the formation of the reaction intermediates and elementary steps at the latter, lower reaction temperatures. To demonstrate that these catalysts can perform the elementary steps required of the Cossee-Arlman mechanism, their ability to activate $H_2$, C-H bonds, and alkylate metal hydrides was evaluated.

# Formation of Metal Hydride Intermediates

Olefin hydrogenation and oligomerization occur at similar temperatures and are thought to form M-H intermediates. *In situ* XAS and IR spectroscopies demonstrate heterolytic dissociation of $H_2$ by single site $Ga^{3+}$ and $Zn^{2+}$ at temperatures where catalytic (hydrogenation) activity is observed. In $H_2$ with increasing temperatures from ambient temperature to 550 °C, there are continual changes in the shape of the Ga (Fig. 2a, 2c, S2a) and Zn (Figure S2c) K-edge XANES. For $Ga/SiO_2$, the white line intensity decreases, and there is formation of a feature before the edge. Changes in XANES were isolated by subtraction of the fresh, unreacted catalyst from that reacted with $H_2$ (Fig. 2b, S2b, S2d), and are due to changes in changes in the coordination geometry and energy of the vacant p-orbitals of the main group metal ion.[26] The magnitude of the $k^2$-weighted EXAFS of the catalysts treated in $H_2$ at elevated temperatures (Fig. 2b, S3) contains a peak at about 1.5 Å (phase uncorrected distance) due to Ga-O or Zn-O bonds. With increasing temperature there is a decrease in the M-O coordination number for both catalysts. M-H bonds are not detected by EXAFS, and the loss of M-O bonds (Table S7) has been suggested to reflect formation of M-H bonds.[24,27,32] There is a loss from 4 to ~ 3 M-O bonds from the fresh to $H_2$ treated catalysts, respectively. In addition, the absence of second shell M-O-M scattering in the EXAFS indicates that the single site structure is maintained at high temperature in $H_2$.

Further evidence for M-H intermediates was investigated by H/D exchange. For example, after treatment of the catalyst with $H_2$, the M-H was reacted with $D_2$ in a temperature programmed surface reaction (TPSR). The normalized HD product corresponds to the fraction of metal hydride sites. For $Ga/SiO_2$, after

$H_2$ treatment at 250 °C, about 0.70 mol HD/mol Ga was formed, which is very similar to the decrease in Ga-O coordination in $H_2$ observed by EXAFS (Fig. 2f, S6, Table S9). The shape of the TPSR profile with increasing reaction temperature is also consistent with only one type of Ga-H species present (Fig. 2e). Similarly, $Zn/SiO_2$ forms 0.19 mol HD/mol Zn at 250 °C, consistent with the changes in coordination number observed in Table S7. Using these fractional surface coverages as a measure of the number of active sites at this temperature, the turnover rates (TOR) can be calculated and are similar for both catalysts (Table S4). Higher reaction temperatures lead to larger amounts of H/D exchange, consistent with a larger number of M-H sites and higher rates (Figure S7, Table S10).

*In situ* IR for $Ga/SiO_2$ also provides evidence for the heterolytic dissociation of $H_2$. The peak at 3745 $cm^{-1}$ corresponds to Si-OH vibrations. Reaction with $H_2$ at increasing temperature from 35 to 550 °C leads to an increased intensity in the Si-OH peak consistent with heterolytic $H_2$ dissociation at Ga-O-Si bonds. Figure 2g show the increase in the intensity of the Si-OH peak with increasing temperature, which was determined by the difference of the spectrum at high temperature to that of the fresh catalyst before $H_2$ reaction.

In addition to an increase in the number of Si-OH, $H_2$ reaction on single site $Ga^{3+}$ also leads to two broad IR peaks at 2034 $cm^{-1}$ and 1875 $cm^{-1}$, which have been previously attributed to Ga-H stretching (Fig. 2h).[38–41] As the temperature increases, the intensity of both peaks increases, consistent with the increase in number of Ga-H sites. The temperature dependence of the IR spectra of Si-OH and Ga-H indicate that $H_2$ dissociation occurs at temperatures as low as 200 °C, which is also the reaction temperature for olefin hydrogenation. Higher temperatures also favor the formation of an increased number of Ga-H sites, as indicated by the larger intensity of these IR bands.

# Alkylation of the Metal Hydride

The reactivity of the M-H with olefins, an elementary reaction of the olefin oligomerization pathway, was also demonstrated by *in situ* XAS. Following formation of Ga-H at 250 °C by reaction with $H_2$, the reacting gas was switched to $C_2H_4$, which led to additional changes in the XANES (Figs. 2a and S4c). The EXAFS also shows a small increase in the first coordination shell, consistent with formation of new M-C bonds (Figs. 2b and S4d). However, the XANES and EXAFS spectra are not identical to the original pre-catalyst suggesting that during the catalytic cycle, both metal hydride and metal alkyl intermediates contribute to the resulting spectra. These changes due to reaction with Ga-H with ethylene were isolated, and a difference analysis was performed to verify the number of new M-C bonds (Figure S5, Table S8).[32,42–45] For example, there are approximately 0.4 and 0.2 Ga-C and Zn-C bonds per metal ion, respectively, by alkylation of the hydrides. In addition, the first shell coordination number remains less than 4 after olefin alkylation suggesting that there are also M-H bonds present, *ca.* 0.4 and 0.5 per $Ga^{3+}$ and $Zn^{2+}$, respectively (Table S7).

Ethylene insertion into the Ga-H was also confirmed by IR giving C-H stretching peaks from 2975 – 2940 $cm^{-1}$ (Figure S8). Thus, $C_2H_4$ insertion into Ga-H and formation of Ga-alkyl is a key elementary step and reaction intermediate characteristic of the Cossee-Arlman mechanism and readily occurs at the same temperature as oligomerization.

# Activation of Ethylene

While reaction of $H_2$ confirms the formation of Ga-H, loss of Ga-O bonds, and formation of Si-OH, *i.e.*, heterolytic dissociation, $H_2$ is not a reactant in olefin oligomerization. Thus, *in situ* IR spectrum of $C_2H_4$ on the $Ga/SiO_2$ pre-catalyst was obtained at temperatures from ambient to 250 °C and gives C-H stretching vibrations between 2975 – 2940 $cm^{-1}$ (Fig. 2i) with many of the same peaks as the Ga-alkyl spectrum (Figure S8). However, with ethylene there is an additional IR peak at 2970 $cm^{-1}$, which was not present in the Ga-alkyl spectra and was previously assigned to a vinyl C-H stretch.[46] The IR spectra suggest that the heterolytic C-H bond dissociation of $C_2H_4$ leads to formation of a Ga-vinyl intermediate at temperatures as low as about 100°C. Higher concentrations are present at 250 °C, where the reaction rate is catalytically relevant. The formation of the M-vinyl intermediate has been proposed by DFT calculations as the initiation reaction in heterogeneous Ni oligomerization catalysts and is an additional elementary step in the heterogeneous oligomerization pathway, which is not required for homogeneous catalysts.[13]

These spectroscopic results demonstrate the formation of reaction intermediates and elementary steps characteristic of the $Ni^{2+}$ Cossee-Arlman reaction mechanism, on these main group elements. Initiation of the catalytic cycle occurs by heterolytic dissociation of C-H bonds of ethylene. The elementary steps and reaction intermediates form at 250°C where catalytic activity is observed, and increasing temperatures lead to higher concentrations of reaction intermediates and higher rates.

# Density Functional Theory Calculations: the $Ga/SiO_2$ Oligomerization Mechanism

A periodic model for single site $Ga^{3+}$ ions in amorphous silica was created by the substitution of Si atoms by Ga. To maintain local charge balance after the substitution, a proton was added to an adjacent oxygen, resulting in an Si-OH moiety. Numerous representative sites, including both three-coordinated (3CN) and four-coordinated (4CN) Ga sites, were considered (Figure S9, S10). 4CN sites exhibit shorter Ga-O bonds, with Si-OH near the active Ga site, and the four Ga-O bonds have an average bond length of 1.89 Å, in agreement with the pre-catalyst structure determined by XAS. Below, we focus on the catalytic properties of these sites. Modeling was done for the initiation steps of the single site $Ga/SiO_2$ pre-catalyst leading to the first reaction intermediate in the catalytic cycle, *i.e.*, Ga-H, followed by calculations for the catalytic pathway.

Initiation of the catalytic cycle begins with heterolytic dissociation of a vinyl C-H bond in $C_2H_4$ across one Ga-O bond. The initial catalyst structure (Fig. 3a) contains a bridging Si-OH, and a second non-bridging Si-OH is formed during the activation of $C_2H_4$. During this process, the Ga-vinyl alkyl C atom develops a

negative charge. The initial ethylene C-H ($sp^2$) bond cleavage has an activation free energy of 1.19 eV. Migratory insertion of $C_2H_4$ into the resulting Ga-vinyl intermediate (2.53 eV), which is likely the rate limiting step, forms a Ga-butenyl intermediate. Subsequent β-H elimination (2.41 eV) leads to stoichiometric amounts of butadiene and a Ga-H intermediate (Figure S11, Table S11). Since one butadiene molecule is formed per Ga site, butadiene was not detected experimentally, but has been proposed based on DFT calculations for $Ni^{2+}$ heterogeneous oligomerization catalysts.[13,14]

An alternate pathway for reaction once the initial $C_2H_4$ activation forms Ga-H, involves dehydration of the two adjacent Si-OH groups. Dehydration is favored due to the low chemical potential of water. Under a water partial pressure of $10^{-9}$ atm, a value that was used in previous silica dehydration studies, the free energy of dehydration is -0.22 eV, which is consistent with results from the prior studies.[47] Dehydration, in turn, leads to slightly more favorable free energies (Figs. 3b, S12, Table S12). The activation free energy of $C_2H_4$ insertion decreases modestly to 2.30 eV (Figure S13); while, the activation barrier of the β-hydride elimination remains nearly unchanged (2.44 eV).

The energy landscape for catalytic oligomerization, beginning with the Ga-H intermediate generated using the dehydrated 4CN Ga model, is illustrated in Fig. 3c, and the structures of the intermediates are given in Fig. 3d (S14-S15, Tables S13-S14). $C_2H_4$ insertion into Ga-H yields a Ga-ethyl intermediate with an activation free energy of 1.85 eV. Subsequent insertion of a second $C_2H_4$ yields a Ga-n-butyl intermediate with activation free energy of 2.54 eV. Finally, β-H elimination (2.57 eV) results in desorption of the olefin product, re-forming of Ga-H, and completing of the catalytic cycle. These energies are similar to those found in previous DFT calculations of $C_3H_8$ dehydrogenation for the β-H elimination of a propyl group on $Zn/SiO_2$.[24]

The oligomerization pathway was also calculated for a less constrained active site, for example, starting from a Ga-H intermediate generated from a 3CN Ga site, which leads to slightly lower activation barriers (Figure S16, Table S15), suggesting that any such minority sites that may be present could also contribute to reactivity. In all cases, the proposed mechanism (Fig. 4) is in line with the Cossee-Arlman scheme that was previously identified for $Ni^{2+}$ ions on zeolite supports.[12,13]

The experimental results demonstrate that $Ga/SiO_2$ has a higher activity than $Zn/SiO_2$, which may be due to lower activation barrier of ethylene insertion and likely contributes to both a higher turnover rate and higher molecular weight in product distribution for Ga-H. It can also be speculated that the activation barrier of β-H elimination is lower on Zn-H site, which allows for earlier termination of ethylene insertion and initiate a new catalytic cycle.

# Discussion

This work demonstrates that isolated, $Ga^{3+}$ and $Zn^{2+}$ ions on $SiO_2$ catalyze olefin oligomerization following the Cossee-Arlman mechanism, which is generally accepted for transition metal catalysts. This

chemistry, however, is unprecedented on main group metal ions. While previously $Ga^{3+}$ ions on solid acid supports, such as MFI (H-ZSM5) zeolite, have been suggested to catalyze olefin oligomerization, the product distributions are characteristic of carbenium ion catalysis, for example, acid catalyzed oligomerization. Skeletal isomerization and cracking are likely from Brønsted acid sites on the zeolite.[48,49] Evidence for oligomerization was suggested based on the IR; however, Brønsted acid sites readily protonate olefins and have similar spectra. Here, the catalytic performance is due to exclusively $Zn^{2+}$ and $Ga^{3+}$ metal ion site, which form linear olefins with even carbon numbers and olefins do not react with the $SiO_2$ support.

Further, this work suggests that at least for single site catalysts, olefin hydrogenation/alkane dehydrogenation and olefin oligomerization are mechanistically related through the formation of the same reaction intermediates and elementary steps. This suggests that any catalyst that is active for one reaction should also be active for the other two if they are structurally stable under all reaction conditions. The single site $Ni^{2+}$, in this study, performs oligomerization; however, $Ni/SiO_2$ reduces to metallic ($Ni^0$) nanoparticles at temperatures higher than about 350 °C, thus is not stable at the high temperature where alkane dehydrogenation is performed.[50] In addition, a recent study demonstrates that single site $Ni^{2+}$ catalysts in Zr-MOF NU1000 catalyze olefin oligomerization and hydrogenation.[51,52] Consistent with this proposal, single site $Cr^{3+}$ is catalytic for alkane dehydrogenation in the Catofin process, and olefin oligomerization, *i.e.*, the Phillips catalyst.[53–57] Thus, there is evidence from heterogeneous transition metal catalysts that all three reactions are mechanistically related.

Based on mechanistic and computational studies of Ni oligomerization catalysts, it is unexpected that main group single site catalysts would have similar chemistries. For example, for Ni, C-C and C-H bond activation requires transfer of electron density from the $C_2H_4$ HOMO to unfilled 3d orbitals, while, Ni 3d electron density is donated to the $C_2H_4$ LUMO, thus forming a π-bond.[20,58] For transition metal catalysts, therefore, the elementary steps (olefin insertion, C-H activation, and β-H elimination) generally involve transition state interactions and bond formation with 3d orbitals. However, main group metals, like $Ga^{3+}$ and $Zn^{2+}$, with $3d^{10}$ electron configurations, would not be expected to participate in these catalytic steps. Thus, the ability of single site $Ga^{3+}$ and $Zn^{2+}$ sites to catalyze oligomerization by the same reaction pathway as $Ni^{2+}$ is unexpected. Nevertheless, as this study shows, the same elementary steps and reaction intermediates are common for $Ni^{2+}$, $Ga^{3+}$, and $Zn^{2+}$. In addition we suggest that hydrogenation/dehydrogenation (Figure S17) and oligomerization reaction pathways (Fig. 4) are related through the formation of the same reaction intermediates (M-H and M-alkyl) and elementary reaction steps (olefin coordination and insertion and β-H elimination). While the specific orbital interactions of these main group active sites with reactants and intermediates remains to be established, the absence of 3d valence orbitals suggests that valence p-orbitals may participate in the catalytic activation, contrary to transition metals where the metal-adsorbate d-orbital bond formation is essential for adsorption, activation, and reaction throughout the catalytic cycle. The results of this study also suggest that other catalytic reactions may be possible with main group elements.

# Conclusion

Main group $Ga^{3+}$ and $Zn^{2+}$ single site catalysts unexpectedly catalyze olefin oligomerization at temperatures as low as 250 °C. Initiation of the catalytic cycle begins by heterolytic dissociation of vinyl C-H bonds of ethylene, for example, and the reaction intermediates and elementary steps suggest a Cossee-Arlman mechanism similar to $Ni^{2+}$ transition metal catalysts. By changing the identity of the main group metal, one can change the resulting product distribution, while, operating with catalytic rates similar to that of $Ni^{2+}$. In addition, unlike $Ni^{2+}$, $Ga^{3+}$ and $Zn^{2+}$ do not reduce to metallic nanoparticles at high temperatures allowing for higher reaction temperatures and are also readily regenerated once deactivated. Overall, this study shows exciting potential for applying main group catalytic sites for several different chemistries, *i.e.*, hydrogenation, dehydrogenation and oligomerization, albeit under different reaction conditions with potential for other catalytic chemistries.

# Methods

Catalyst Preparation. Single site $Ga/SiO_2$ and $Zn/SiO_2$ were prepared following the procedures previously reported in literature, using standard catalyst synthesis techniques, and compared to a $Ni/SiO_2$ control.[23,24,50]

$Ga/SiO_2$ was synthesized with a chelating agent to prevent the formation of $Ga_2O_3$ using pH-controlled incipient wetness impregnation (IWI). 10 g of Davisil silica with grade 636 (pore size = 60 Å, surface area = 480 $m^2/g$) was impregnated with an aqueous solution containing 1.5 g of gallium nitrate solution ($Ga(NO_3)_3$ $xH_2O$, Fluka chemical) and 1.5 g of citric acid (Sigma Aldrich) dissolved in Millipore water. The catalyst was dried for 16 hours at 125 °C and then calcined at 500 °C for 3 hours. Atomic absorption spectroscopy (AAS) was used to determine that the final catalyst contained approximately 2.6 wt% Ga.

$Zn/SiO_2$ was synthesized using pH-controlled strong electrostatic adsorption (SEA). A solution containing 2.5 g of zinc nitrate hexahydrate ($Zn(NO_3)_2$ $6H_2O$, Sigma Aldrich) was made and the pH was adjusted to 11 using 30% ammonium hydroxide ($NH_4OH$) solution, until a clear solution was obtained. 10 g of Davisil silica was suspended 100 mL of Millipore water in a separate beaker and the pH was adjusted to 11 using $NH_4OH$. The Zn solution was added rapidly to the $SiO_2$ solution and stirred for 20 minutes. After the solid was settled, the solution was decanted, and the resulting slurry was washed with Millipore water and collected by vacuum filtration. The catalyst was dried for 16 hours at 125 °C and then calcined at 300 °C for 3 hours. AAS was used to determine that the final catalyst contained approximately 4.0 wt% Zn.

$Ni/SiO_2$ was prepared by pH-controlled SEA. A solution containing 3.0 g of nickel nitrate hexahydrate ($Ni(NO_3)_2$ $6H_2O$) was prepared and the pH was adjusted to 11 using 30% $NH_4OH$ solution until a clear blue solution was obtained. 10 g of Davisil silica was added to the solution and the suspension was stirred for 20 minutes. At the end of the reaction, additional $NH_4OH$ was added to the solution to maintain

a pH of 11. The suspension was stirred for another 10 minutes before being filtered and the catalyst was recovered. The catalyst was dried for 16 hours at 125 °C and then calcined at 300 °C for 3 hours. AAS was used to determine that the final catalyst contained approximately 2.7 wt% Ni.

Catalyst Testing. Oligomerization tests were performed at atmospheric pressure in pure ethylene or pure propylene using a fixed bed reactor of 3/8-inch OD. The weight of catalyst loaded into the reactor ranged from 0.5 g to 1 g and was diluted with silica to reach a total of 1 g. The catalyst was treated in 50 ccm of $N_2$ while it ramped to 250 °C for the reaction. The reaction was performed in 100% $C_2H_4$ using GHSVs ranging from 0.08 $s^{-1}$ to 0.38 $s^{-1}$. Products from the atmospheric pressure reactor were analyzed with a Hewlett Packard (HP) 6890 Series gas chromatograph (GC) using a flame ionization detector (FID) with an Agilent HP-Al/S column (25 m in length, 0.32 mm ID, and 8 μm film thickness).

High pressure oligomerization was performed in a stainless steel, fixed bed reactor of 1/2-inch OD. 2 g of catalyst was loading into the reactor. The reactor was pressurized to 450 psig (30.6 atm) and the catalyst was treated in 50 ccm of $N_2$ while it ramped to 250 °C for the reaction. The reaction was performed in a mixture of 10 ccm 5% $CH_4/N_2$ for an internal standard and 50 ccm 100% $C_2H_4$ at a total pressure of 450 psig. Products were analyzed with a Hewlett Packard (HP) 7890 Series gas chromatograph (GC) using a flame ionization detector (FID) with an Agilent HP-1 column (60 m in length, 0.32 mm ID, and 25 μm film thickness).

Characterizations.

*In Situ X-ray Absorption Spectroscopy (XAS)*

*In-situ* XAS was performed at the Ga K (10.3670 keV), Zn K (9.659 keV), and Ni K (8.333 keV) edges at the 10-BM sector at the Advanced Photon Source at Argonne National Laboratory using transmission mode with scan ranges from 250 keV below the edge to 800 keV above the edge. At the Ga K edge, the samples were calibrated to $Ga_2O_3$ (10.3751 keV). Samples were pressed into a stainless-steel sample holder and placed in a quartz-tube sample cell with gas flow capabilities. The structure of each catalyst was studied after dehydration at 550 °C in He. The sample cell was cooled to room temperature and scanned. The resulting structure of each was compared to known references including Ga acetylacetonate ($Ga(AcAc)_3$), Ga oxide ($Ga_2O_3$), Zn oxide (ZnO), and Ni oxide (NiO) to confirm the oxidation state and coordination environment (*i.e.* coordination number and bond distance). The data was processed using the WinXAS v.3.1 software[59] to find the coordination number and bond distance using standard procedures. Feff6 calculations were performed using $Ga_2O_3$ (50% at CN = 4, R = 1.83 Å and 50% CN = 6 at 2.00 Å), ZnO (CN = 4, R = 1.98 Å), and NiO (CN = 6, R = 2.09 Å) respectively for reference. A least squared fit for the first shell of r-space and isolated q-space were performed on the $k^2$ weighted Fourier transform data over the range of 2.7 to 10 $Å^{-1}$ in each spectrum to fit the magnitude and imaginary components.

An understanding of reactive intermediates was obtained on $Ga/SiO_2$ and $Zn/SiO_2$ using *in situ* XAS. A furnace was placed on the beamline around the sample cell to allow for structural measurements at high

temperature. Data was continuously collected as the temperature ramped in pure $H_2$ to 550 °C. Once the structure was stabilized (*i.e.* the resulting XAS spectra remained unchanged), the cell was cooled to 250 °C in pure $H_2$ while scanning continuously. When the structure was stabilized, the temperature was held constant at 250 °C and the gas flow was switched from pure $H_2$ to pure $C_2H_4$. Measurements in He were also obtained at 250 °C and 550 °C. The XANES were used to determine the oxidation state and geometry while select EXAFS spectra were used to determine the coordination number and bond distances of the M-O bonds (M = Ga, Zn).

*H/D Isotope Exchange Experiments*

To confirm the formation of the metal hydride intermediates and count the number of active metal hydride sites that form, a $H_2/D_2$ isotopic exchange experiment was performed using a Micromeritics Autochem II 2920 chemisorption analyzer, equipped with a residual gas analyzer (RGA). Calibrations for the $H_2$, $D_2$, and HD signal were performed in a bypass line while the sample was being dehydrated at 500 °C in inert gas. For the HD calibration, two separate gas mixtures containing 5% $H_2$/95% Ar and 5% $D_2$/95% Ar were combined in different relative amounts in a bypass line to measure initial feed $H_2/D_2$ ratios in balance Ar compositions. Samples were loaded into a quartz U-tube reactor and treated in flowing air for dehydration at 500 °C before being cooled to 250 °C. The sample was exposed to 5% $H_2$/Ar for 1 hour and then switched to 5% $D_2$/Ar while the signals for $H_2$, $D_2$ and HD were recorded on the RGA. During this time, the $H_2$ signal returned to its baseline, the $D_2$ signal increased to its feed value, and the HD signal increased immediately and decreased with time as $D_2$ reacted with H atoms in metal hydrides to form HD and metal deuterides. Once the HD signal reached baseline values, the gas flow was switched from 5% $D_2$/Ar to 5% $H_2$/Ar to quantify the HD formed in the reverse isotopic exchange experiment, and this was repeated for a total of four switches and averaged to estimate the number of metal-hydride sites present.

$H_2/D_2$ isotopic exchange in a temperature programmed surface reaction (TPSR) was performed to identify the number of different metal specific in a catalyst. First, the catalyst was dehydrated at 500 °C treated in air for 2 h. Then, the sample was cooled to 450 °C in air. The catalyst was treated in 5% $H_2$/95% Ar at 450 °C for 2 h. The temperature was cooled to ambient in 5% $H_2$/95% Ar. Then, 5% $H_2$/95% Ar was switched to 5% $D_2$/95% Ar and the temperature was increased from 35 to 900 °C.

*Fourier Transform Infrared Spectroscopy (FT-IR)*

Infrared (IR) spectra were collected using a Nicolet 4700 spectrometer with a Hg-Cd-Te detector (MCT, maintained at -196 °C by liquid $N_2$). Each spectrum represents the average of 64 scans at 2 $cm^{-1}$ resolution from 4000 to 400 $cm^{-1}$ and were taken using an empty cell background reference (30 °C) collected under dynamic vacuum (rotary vane rough pump, Alcatel 2008A, < 0.01 kPa). In a typical experiment, 0.02–0.04 g $cm^{-2}$ of sample were pressed into self-supporting wafers of $Ga/SiO_2$ and held in a custom-built quartz IR cell with $CaF_2$ windows. IR cells were inserted into a mineral-insulated heating

coil (ARi Industries) contained within an alumina silicate ceramic chamber (Purdue Research Machining Services). The quartz IR cell was connected to a glass vacuum manifold that was used for sample pretreatment and exposure to gas-phase, pure ethylene. When the $Ga/SiO_2$ sample was loaded, it was dehydrated in He at 550 °C for 2 h and a spectrum of the dehydrated sample was obtained. Then, the catalyst was cooled to ambient temperature and exposed to pure $H_2$. The temperature was ramped to 550 °C in pure $H_2$ at a rate of 10 °C/min while spectra were collected every 5 minutes. The temperature was held at 550 °C in pure $H_2$ for 1 h and then cooled to ambient temperature. The gas was switched to pure $C_2H_4$ and the temperature was ramped at 10 °C/min to 250 °C, while collecting spectra every 5 minutes. The temperature was held at 250 °C for 2 h. A second $Ga/SiO_2$ wafer was prepared and dehydrated using the same method as detailed above. The catalyst was cooled to ambient temperature and exposed directly to pure $C_2H_4$. The temperature was ramped at 10 °C/min to 250 °C while collecting spectra every 5 minutes, and the $C_2H_4$ treated sample spectra were compared the sample with and without $H_2$ pretreatment. IR spectra reported here were baseline corrected, and the spectra shown are difference spectra with that of the dehydrated catalyst subtracted from those of the treated catalysts.

*Density Functional Theory (DFT)*

$Ga/SiO_2$ systems are based on a recently developed amorphous silica model using molecular dynamics and continuous dehydration processes.[56] A periodic amorphous silica model (21.6 Å × 21.6 Å × 34.5 Å; 372 atoms) was used to analyze the energetics of Ga-H formation and ethylene oligomerization. Ga sites were generated by substituting Si atoms and adding a proton to maintain charge balance. All DFT calculations are performed with self-consistent and periodic density functional theory using the Vienna Ab-initio Simulation Package (VASP).[60–64] The BEEF-VdW exchange-correlation functional[65], using projector augmented wave (PAW) pseudopotentials[64,66], was employed. A dipole correction was applied parallel to the plane of the slab to reduce image interaction errors. A *k* point grid of 2 × 2 × 1 was used based on Monkhorst-Pack *k*-sampling. A cutoff energy of 400 eV and a force-convergence criterion of 20 meV $Å^{-1}$ for local minima were considered. Transition state geometries were obtained through a climbing-image nudged-elastic-band (NEB) method[67,68], where for each elementary step, seven images were generated as the initial guesses using the Image Dependent Pair Potential pre-optimizer.[69] After an NEB calculation was converged, where the force exerted on each image was below 100 meV $Å^{-1}$, the LANCZOS diagonalization approach was employed to locate the transition state with a force-convergence criterion of 80 meV $Å^{-1}$.[70] The harmonic vibrational states were used for zero-point vibrational energy corrections ($E_{ZPE}$), and these also formed the basis for estimating entropies of the adsorbates. However, for the vibration modes with low wave numbers (< 150 $cm^{-1}$), particle-in-a-box (PIB) and free rotor schemes were used for calculating their contributions to the entropies, depending on the geometric characteristics of the vibration (see Supporting Information for an example). Free energies, evaluated at 250 °C, were obtained using the following equation: $G = E_{DFT} + E_{ZPE} - TS$, where $E_{DFT}$ is the ground-state potential energy calculated using DFT. The calculation of adsorption energy ($G_{ads}$) use the reference site energy ($G_{Ga}$), which can either be an empty Ga site or Ga hydride, and the gaseous ethylene

molecule at 1 atm ($G_{ethylene}$): $G_{ads} = G_A - G_{Ga} - X \times G_{ethylene}$, where $X$ is a stoichiometrically appropriate number of reference ethylene molecules.

## Declarations

# AUTHOR CONTRIBUTIONS

The project was conceived by N.L, J.T.M, and G.Z. Catalysts preparation and testing was performed by N.L, A.Q, E.E., and R.N. N.L. performed *in situ* XAS measurements and structural analysis. FTIR was performed by J.C.V.V under the supervision of R.G. Isotopic exchange experiments were performed by A.S. under the supervision of R.G. Y.X. conducted mechanism analysis via DFT calculations under the supervision of J.G.

# ACKNOWLEDGEMENTS

This work was supported by the National Science Foundation under Cooperative Agreement no. EEC1647722. G.Z. would like to acknowledge the National Natural Science Foundation of China (21902019) and Fundamental Research Funds for the Central Universities (DUT18RC(3)057 and DUT20RC(5)002). Use of the Center for Nanoscale Materials and Advanced Photon Source, both Office of Science user facilities, was supported by the U.S. Department of Energy, Office of Science, Office of Basic Energy Sciences, under Contract No. DE-AC02-06CH11357. MRCAT operations and the beamline 10-BM were supported by the Department of Energy and the MRCAT member institutions. Information Technology at Purdue (West Lafayette, IN), and computational resources from the National Energy Research Scientific Computing Center is gratefully acknowledged.

## References

1. Sydora, O.L. Selective Ethylene Oligomerization. *Organometallics*. 2019, 38, 997–1010.
2. Lavrenov, A.V.; Karpova, T.R.; Buluchevskii, E.A.; Bogdanets, E.N. Heterogeneous oligomerization of light alkenes: 80 years in oil refining. *Catal. Ind.* 2016, 8, 316–327.
3. Keim, W. Nickel: An Element with Wide Application in Industrial Homogeneous Catalysis. 1990, 29, 235–244.
4. Forestière, A.; Olivier-Bourbigou, H.; Saussine, L. Oligomerization of Monoolefins by Homogeneous Catalysts. *Oil & Gas Science and Technology - Rev. IFP* 2009, 64, 649–667.
5. Keim, W. Oligomerization of Ethylene to α-Olefins: Discovery and Development of the Shell Higher Olefin Process (SHOP). *Angewandte Chemie.* 2013, 52,12492–6.
6. Al-Jarallah, A. M.; Anabtawi, J. A.; Siddiqui, M. A. B.; Aitani, A. M.; Al-Sa'doun, A. W. Ethylene dimerization and oligomerization to butene-1 and linear α-olefins: A review of catalytic systems and processes. *Catalysis Today.* 1992, 14, 1–121.

7. Mathys, G. M. K.; Martens, L. R. M.; Baes, M. A., Verduijn, J. P.; Huybrechts, D. R. C. 1997. Alkene oligomerization. US Patent 20040006250, filed April 14, 2003, and issued January 8, 2004.
8. Brown, S. H.; Godsmark, J. S.; Mathys, G. M. K. 2010. Olefin oligomerization process. US Patent 20070173676A1, filed June 1, 2004, and issued August 31, 2010.
9. Verrelst, W. H.; Martens, L. R. M. 1995. Oligomerization and catalysts therefor. French Patent WO1995022516A1, filed February 22, 1994, and issued August 24, 1995.
10. Finiels, A.; Fajula, F.; Hulea, V. Nickel-based solid catalysts for ethylene oligomerization – a review. *Catal. Sci. Technol.* 2014, 4, 2412–2426.
11. Killian, C. M.; Johnson, L. K.; Brookhart, M. Preparation of Linear α-Olefins Using Cationic Nickel(II) α-Diimine Catalysts. *Organometallics*. 1997, 16, 2005–2007.
12. Joshi, R., Zhang, G., Miller, J. T. & Gounder, R. Evidence for the Coordination–Insertion Mechanism of Ethene Dimerization at Nickel Cations Exchanged onto Beta Molecular Sieves. *ACS Catal*. 2018, 8, 11407–11422.
13. Brogaard, R. Y.; Olsbye, U. Ethene Oligomerization in Ni-Containing Zeolites: Theoretical Discrimination of Reaction Mechanisms. *ACS Catal.* 2016, 6, 1205–1214.
14. Henry, R.; Komurcu, M.; Ganjkhanlou, Y.; Brogaard, R.Y.; Lu, L.; Jens, K.J.; Berlier, G.; Olsbye, U. Ethene oligomerization on nickel microporous and mesoporous-supported catalysts: Investigation of the active sites. *Catalysis Today*, 2018, 9, 154–163.
15. Nicholas, C. P. Applications of light olefin oligomerization to the production of fuels and chemicals. *Applied Catalysis A: General*, 2017, 543, 82–97.
16. Moussa, S.; Concepción, P.; Arribas, M. A.; Martínez, A. Nature of Active Nickel Sites and Initiation Mechanism for Ethylene Oligomerization on Heterogeneous Ni-beta Catalysts. *ACS Catal*. 2018, 8, 3903–3912.
17. Martínez, A.; Arribas, M. A.; Concepción, P.; Moussa, S. New bifunctional Ni–H-Beta catalysts for the heterogeneous oligomerization of ethylene. *Applied Catalysis A: General*, 2013, 467, 509–518.
18. McGuiness, D.S. Olefin Oligomerization via Metallacycles: Dimerization, Trimerization, Tetramerization, and Beyond. *Chemical Reviews*, 2011, 111, 2321–2341.
19. Biscardi, J. A.; Meitzner, G. D.; Inglesia, E. Structure and Density of Active Zn Species in Zn/H-ZSM5 Propane Aromatization Catalysts. *Journal of Catalysis*, 1998, 179, 192–202.
20. La, M.-J.; Wang, Y-C.; Wang, C-L.; Ji, D-F.; Jin, Y-Z.; Nian, J-Y.; Ma, W-P. The DFT study on CC activation of butanone by Ni + in gas phase: Two parallel decomposition reaction mechanisms. *Computational and Theoretical Chemistry*. 2012, 979, 128–134.
21. Forget, S.; Olivier-Bourbigou, H.; Delcroix, D. Homogeneous and Heterogeneous Nickel-Catalyzed Olefin Oligomerization: Experimental Investigation for a Common Mechanistic Proposition and Catalyst Optimization. *ChemCatChem*, 2017, 9, 2408–2417.
22. Phadke, N. M.; Van der Mynsbrugge, J.; Mansoor, E.; Getsoian, A.B.; Head-Cordon, M.; Bell, A.T. Characterization of Isolated Ga3 + Cations in Ga/H-MFI Prepared by Vapor-Phase Exchange of H-MFI

Zeolite with GaCl3. *ACS Catal*. 2018, 8, 6106–6126.

23. Cybulskis, V. J.; Pradhan, S.U.; Lovon-Quintana, J.J.; Hock, A.S.; Hu, B.; Zhang, G.; Delgass, W.N.; Ribeiro, F.H.; Miller, J.T. The Nature of the Isolated Gallium Active Center for Propane Dehydrogenation on Ga/SiO2. *Catal Lett*.2017, 147, 1252–1262.
24. Schweitzer, N. M.; Hu, B.; Das, U.; Kim, H.; Greeley, J.; Curtiss, L.A.; Stair, P.C.; Miller, J.T.; Hock, A.S. Propylene Hydrogenation and Propane Dehydrogenation by a Single-Site Zn2 + on Silica Catalyst. *ACS Catal*. 2014, 4, 1091–1098.
25. Pidko, E. A.; Hensen, E. J. M.; van Santen, R. A. Dehydrogenation of Light Alkanes over Isolated Gallyl Ions in Ga/ZSM-5 Zeolites. *J. Phys. Chem. C.* 2007, 111, 13068–13075.
26. Schreiber, M. W.; Plaisance, C.P.; Baumgartl, M.; Reuter, K.; Jentys, A.; Bermejo-Deval, R.; Lercher, J.A. Lewis–Brønsted Acid Pairs in Ga/H-ZSM-5 To Catalyze Dehydrogenation of Light Alkanes. *J. Am. Chem. Soc*. 2018, 140, 4849–4859.
27. Hu, B.; Getsoian, A.B.; Schweitzer, N.M.; Das, U.; Kim, H.; Niklas, J.; Poluektov, O.; Curtiss, L.A.; Stair, P.; Miller, J.T.; Hock, A.S. Selective propane dehydrogenation with single-site CoII on SiO2 by a non-redox mechanism. *Journal of Catalysis*. 2015, 322, 24–37.
28. Hu, B.; Getsoian, A.B.; Schweitzer, N.M.; Das, U.; Zhang, G.; Kraft, S.J.; Childers, D.J.; Lanci, M.P.; Miller, J.T.; Hock, A.S.. Isolated FeII on Silica As a Selective Propane Dehydrogenation Catalyst. *ACS Catalysis.* 2015, 5, 3494–3503.
29. Szeto, K. C.; Gallo, A.l Hernandez-Morejudo, S.; Olsbye, U.; Selective Grafting of Ga(i-Bu)3 on the Silanols of Mesoporous H-ZSM-5 by Surface Organometallic Chemistry. *J. Phys. Chem. C*. 2015, 119, 26611–26619.
30. Taha, Z. A.; Deguns, E.W.; Chattopadhyay, S.; Scott, S. L. Formation of Digallium Sites in the Reaction of Trimethylgallium with Silica. *Organometallics*. 2006, 25, 1891–1899.
31. Fleischman, S. D.; Scott, S. L. Evidence for the Pairwise Disposition of Grafting Sites on Highly Dehydroxylated Silicas via Their Reactions with Ga(CH3)3. *J. Am. Chem. Soc.* 2011, 133, 4847–4855.
32. Getsoian, A.B.; Das, U.; Camacho-Bunquin, J.; Zhang, G.; Gallagher, J.R.; Hu, B.; Cheah, S.; Schaidle, J.A.; Ruddy, D.A.; Hensley, J.E.; Krause, T.R.; Curtiss, L.A.; Miller, J.T.; Hock, A.S. Organometallic model complexes elucidate the active gallium species in alkane dehydrogenation catalysts based on ligand effects in Ga K-edge XANES. *Catalysis Science & Technology*. 2016, 6, 6339–6353.
33. Britovsek, G. J. P.; Malinowski, R.; McGuinness, D.S.; Nobbs, J.D.; Tomov, A.K.; Wadsley, A.W.; Young, C.T. Ethylene Oligomerization beyond Schulz – Flory Distributions. *ACS Catal*. 2015, 4, 6922–6925.
34. Metzger, E. D.; Comito, R. J.; Hendon, C. H.; Dincă, M. Mechanism of Single-Site Molecule-Like Catalytic Ethylene Dimerization in Ni-MFU-4 l. *J. Am. Chem. Soc*. 2017, 139, 757–762.
35. Bartlett, B.; Hossain, M. M.; Tysoe, W. T. Reaction Pathway and Stereoselectivity of Olefin Metathesis at High Temperature. *Journal of Catalysis*. 1998, 176, 439–447.
36. Choi, S.W.; Kim, W-G.; So, J-S.; Moore, J.S.; Liu, Y.; Dixit, R.S.; Pendergast, J.G.; Sievers, C.; Sholl, D.S.; Nair, S.; Jones, C.W. Propane dehydrogenation catalyzed by gallosilicate MFI zeolites with perturbed

acidity. *Journal of Catalysis*. 2017, 345, 113–123.

37. *Catal. Sci. Technol.*, **2019**, 9, 2812–2827.
38. Collins, S.E.; Baltanás, M. A.; Bonivardi, A. L. Hydrogen Chemisorption on Gallium Oxide Polymorphs. *Langmuir*. 2005, 21, 962–970.
39. Rodrigues, V. de O.; Faro Júnior, A. C. On catalyst activation and reaction mechanisms in propane aromatization on Ga/HZSM5 catalysts. *Applied Catalysis A: General*. 2012, 5, 68–77.
40. Serykh, A. I. On the formation of surface gallium hydride species in supported gallium catalysts. *Applied Surface Science*. 2012, 259, 252–255.
41. Almutairi, S. M. T.; Mezari, B.; Magusin, P. C. M. M.; Pidko, E. A.; Hensen, E. J. M. Structure and Reactivity of Zn-Modified ZSM-5 Zeolites: The Importance of Clustered Cationic Zn Complexes. *ACS Catal*. 2012, 2, 71–83.
42. LiBretto, N.J.; Yang, C.; Ren, Y.; Zhang, G.; Miller, J.T. Identification of Surface Structures in Pt3Cr Intermetallic Nanocatalysts. *Chemistry of Materials*, 2019, 31, 1597–1609.
43. Mijovilovich, A. Delta-mu XANES reveals the electronic structure of the adsorption of propene on gold nanoparticles. *RSC Adv.*, 2014, 4, 12293–12297.
44. Bus, E.; Ramaker, D.E.; van Bokhoven, J.A. Structure of Ethene Adsorption Sites on Supported Metal Catalysts from in Situ XANES Analysis. *J. Am. Chem. Soc.*, 2007, 129, 8094–8102.
45. Goulon, J.; Friant, P.; Goulon-Ginet, C.; Coutsolelos, A.; Guilard, R. Bridge-stacked polymeric structure of a fluorinated Ga(III) porphyrin deduced from a perturbed difference fourier analysis of EXAFS spectra. *Chemical Physics*, 1984, 83, 367–375.
46. Kazansky, V. B.; Pidko, E. A. Intensities of IR Stretching Bands as a Criterion of Polarization and Initial Chemical Activation of Adsorbed Molecules in Acid Catalysis. Ethane Adsorption and Dehydrogenation by Zinc Ions in ZnZSM-5 Zeolite. *J. Phys. Chem. B.* 2005, 109, 2103–2108.
47. Comas-Vives, A. Amorphous SiO2 surface models: energetics of the dehydroxylation process, strain, ab initio atomistic thermodynamics and IR spectroscopic signatures. *Phys. Chem. Chem. Phys*. 2016, 18, 7475–7482.
48. Pidko, E.A.; Hensen, E.J.M.; van Santen, R.A. Anionic Oligomerization of Ethylene over Ga/ZSM-5 Zeolite: A Theoretical Study. *J. Phys. Chem. C*. 2008, 112, 19604–19611.
49. Kuz´min, I.V.; Sokolova, N.A.; Subbotina, I.R.; Zhidomirov, G.M. Ethylene adsorption and transformation on zeolite Ga+/ZSM-5. *Russ Chem Bull*. 2015, 64, 278–283.
50. Zhang, G.; Yang, C.; Miller, J. T. Tetrahedral Nickel(II) Phosphosilicate Single-Site Selective Propane Dehydrogenation Catalyst. *ChemCatChem*. 2017, 10, 961–964.
51. Shabbir, H.; Pellizzeri, S.; Ferradon, M.; Kim, I.S.; Vermeulen, N.A.; Farha, O.K.; Delferro, M.; Martinson, A.; Getmen, R.B. Influence of Spin State and Electron Configuration on the Active Site and Mechanism for Catalytic Hydrogenation on Metal Cation Catalysts Supported on NU-1000: Insights from Experiments and Microkinetic Modeling. *Catal. Sci. Technol*. 2020.

52. Li, Z; Schweitzer, N.M.; League, A.B.; Bernales, V.; Peters, A.W.; Getsoian, A.B.; Wang, T.C.; Miller, J.T; Vjunov, A.; Fulton, J.L.; Lercher, J.A.; Cramer, C.J.; Gagliardi, L.; Hupp, J.T.; Farha, O.K. Sintering-Resistant Single-Site Nickel Catalyst Supported by Metal–Organic Framework. *J. Am. Chem. Soc.* 2016, 138, 1977–1982.
53. Agapie, T. Selective ethylene oligomerization: Recent advances in chromium catalysis and mechanistic investigations. *Coordination Chemistry Reviews*, 2011, 255, 861–880.
54. Alferov, K.A.; Belov, G.P.; Meng, Y. Chromium catalysts for selective ethylene oligomerization to 1-hexene and 1-octene: Recent results. *Applied Catalysis A: General*, 2017, 542, 71–124.
55. Cheng, Y.; Zhou, L.; Xu, J.; Miao, C.; Hua, W.; Yue, Y.; Gao, Z. Chromium-based catalysts for ethane dehydrogenation: Effect of SBA-15 support. *Microporous and Mesoporous Materials*, 2016, 234, 370–376.
56. Floryan, L.; Borosy, A. P.; Núñez-Zarur, F.; Comas-Vives, A.; Copéret, C. Strain effect and dual initiation pathway in CrIII/SiO2 polymerization catalysts from amorphous periodic models. *Journal of Catalysis*. 2017, 346, 50–56.
57. Conley, M. P.; Delley, M. F.; Núñez-Zarur, F.; Comas-Vives, A.; Copéret, C. Heterolytic Activation of C-H Bonds on Cr(III)-O Surface Sites Is a Key Step in Catalytic Polymerization of Ethylene and Dehydrogenation of Propane. *Inorg Chem*. 2015, 54, 5065–5078.
58. Trofymchuk, O.S.; Ortega, D.E.; Gutiérrez-Oliva, S.; Rojas, R.S.; Toro-Labbé, A. The performance of methallyl nickel complexes and boron adducts in the catalytic activation of ethylene: a conceptual DFT perspective. *J Mol Model*. 2015, 21, 227.
59. Ressler, T. WinXAS: a Program for X-ray Absorption Spectroscopy Data Analysis under MS-Windows. *J. Synchrotron Rad.* 1998. 5, 118–122.
60. Kresse, G.; Furthmüller, J. Efficiency of ab-initio total energy calculations for metals and semiconductors using a plane-wave basis set. *Computational Materials Science*. 1996, 6, 15–50.
61. Kresse, G.; Furthmüller, J. Efficient iterative schemes for ab initio total-energy calculations using a plane-wave basis set. *Phys. Rev. B.* 1996, 54, 11169–11186.
62. Kresse, G.; Hafner, J. Ab initio molecular dynamics for liquid metals. *Phys. Rev. B.* 1993, 47, 558–561.
63. Kresse, G.; Hafner, J. Ab initio molecular-dynamics simulation of the liquid-metal–amorphous-semiconductor transition in germanium. *Phys. Rev. B*. 1994, 49, 14251–14269.
64. Kresse, G.; Joubert, D. From ultrasoft pseudopotentials to the vas projector augmented-wave method. *Phys. Rev. B*. 1999, 59, 1758–1775.
65. Wellendorff, J.; Lundgaard, K.T.; Mogelhoj, A.; Petzold, V.; Landis, D.D.; Norskov, J.K.; Bligaard, T.; Jacobsen, K.W. Density functionals for surface science: Exchange-correlation model development with Bayesian error estimation. *Phys. Rev. B*. 2012, 85, 235149.
66. Blöchl, P. E. Projector augmented-wave method. *Phys. Rev. B*. 1994, 50, 17953–17979.
67. Henkelman, G.; Jónsson, H. Improved tangent estimate in the nudged elastic band method for finding minimum energy paths and saddle points. *J. Chem. Phys.* 2000, 113, 9978–9985.

68. Henkelman, G.; Uberuaga, B.P.; Jónsson, H. A climbing image nudged elastic band method for finding saddle points and minimum energy paths. *J. Chem. Phys.* 2000, 113, 9901–9904.
69. Smidstrup, S.; Pedersen, A.; Stokbro, K.; Jónsson, H. Improved initial guess for minimum energy path calculations. *J. Chem. Phys.* 2014, 140, 214106.
70. Olsen, R.A.; Kroes, G.J.; Henkelman, G.; Arnaldsson, A.; Jónsson, H. Comparison of methods for finding saddle points without knowledge of the final states. *J. Chem. Phys.* 2004, 121, 9776–9792.

## Scheme

Scheme 1 is available in the Supplementary Files

## Figures

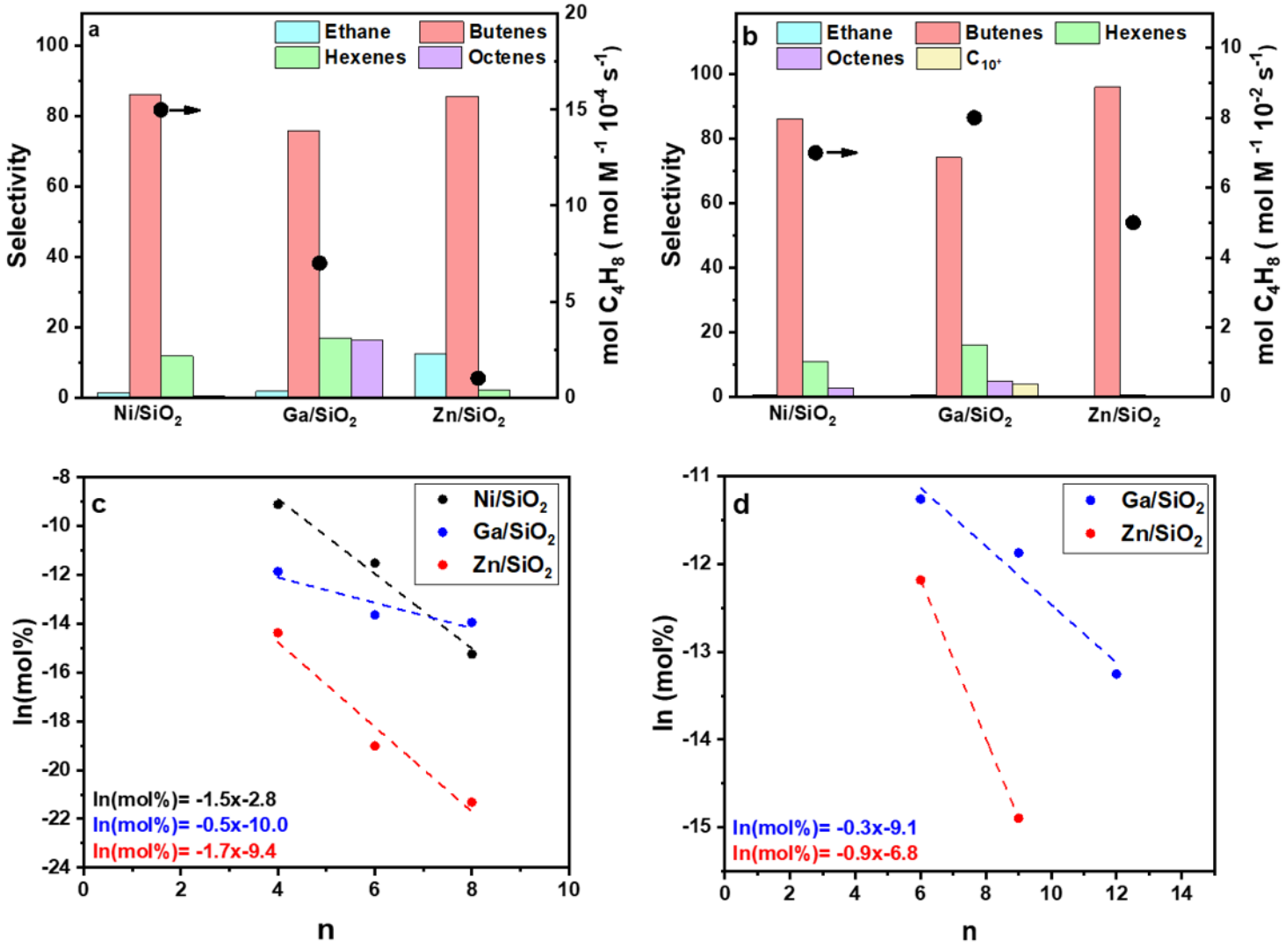


Figure 1

Ethylene Oligomerization Performance. a,b) Product distribution and reaction rate for C2H4 oligomerization at 250°C, 1 atm (X= ~5%) (a) and 30.6 atm (X = ~20%) (b) c,d) Schultz Flory distributions shown by dashed lines for oligomerization in C2H4 (c) and C3H6 (d)

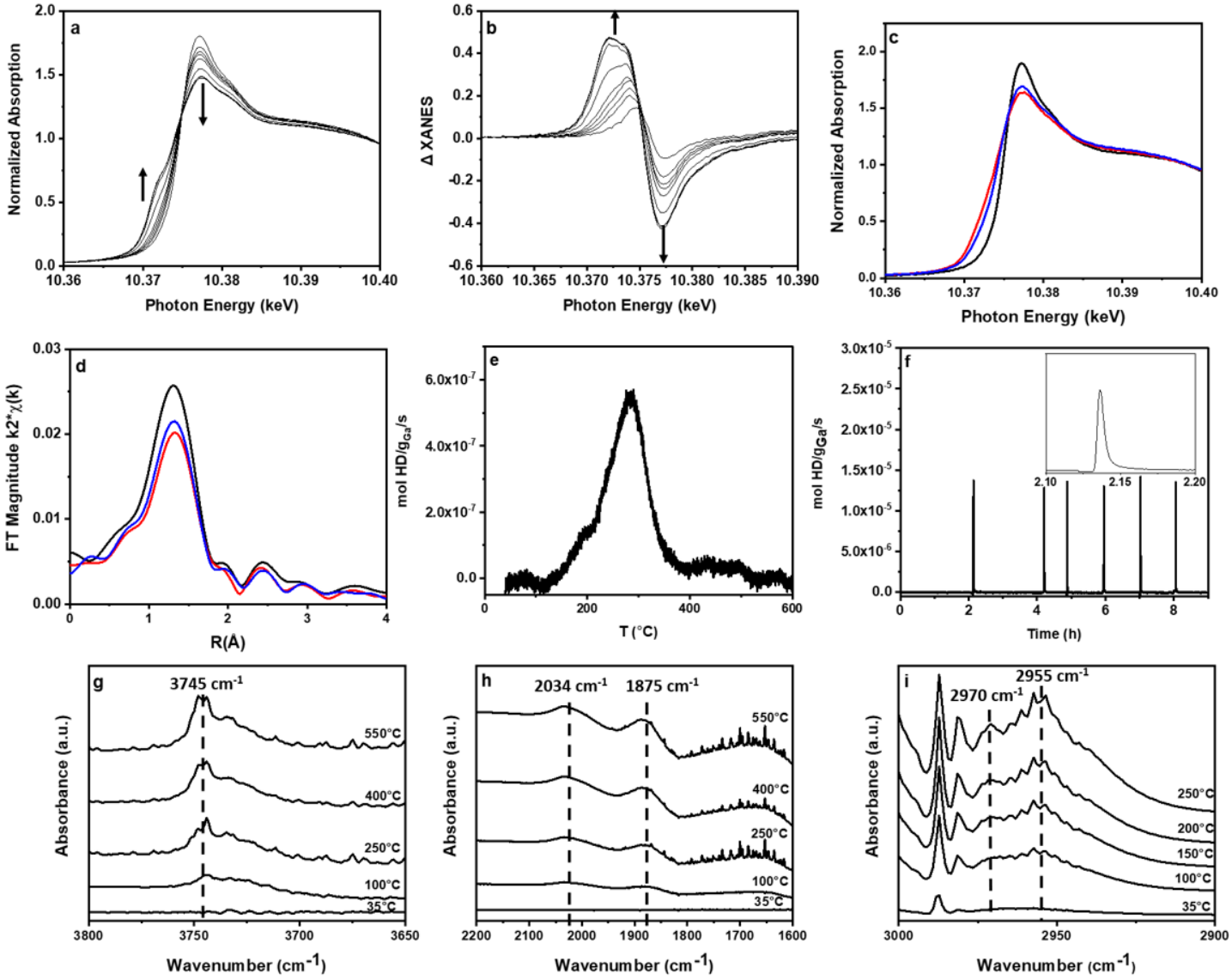


## Figure 2

Characterization of active intermediates on Ga/SiO2 a,b) Normalized Ga K edge XANES (a) and EXAFS (b) demonstrates increasing spectroscopic changes with increasing temperature in H2, where arrows lead to higher reaction temperature c,d) Normalized Ga K edge XANES (c) and EXAFS (d) demonstrates that alkylation (blue) of the metal hydride (red) leads to restoration of the pre-catalyst structure (black) on Ga/SiO2 e) HD formation rates from M-H/D2 isotopic exchange in TPSR f) time on stream for gaseous HD formation g,h) IR O-H stretching region for Ga/SiO2 after treatment in pure H2 at increasing temperature from 35°C to 550°C, shown as a difference spectrum between the H2-treated and the dehydrated catalyst for the 3800-3650 cm-1 region corresponding to Si-OH stretching (g) and the 2200-1600 cm-1 region corresponding to Ga-H stretching (h) i) the C-H stretching region for Ga/SiO2 after

treatment in pure C2H4 at increasing temperature from 35°C to 250°C shown as a difference spectrum between that under C2H4 exposure and the dehydrated catalyst.

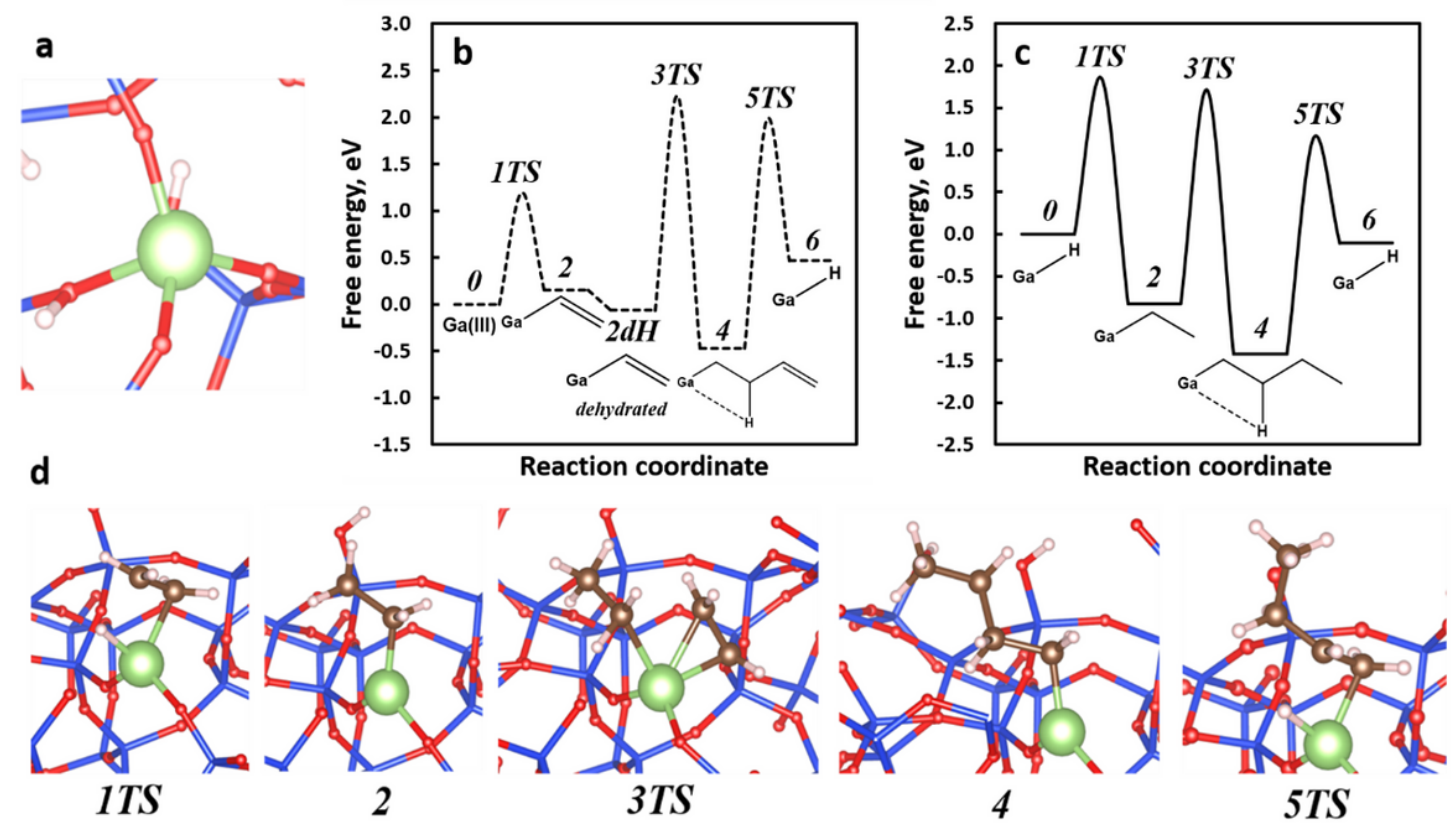


## Figure 3

Activation and oligomerization on Ga/SiO2. a) Ga site model where Ga=green, O=red, Si=blue, and H=white b) Free energy diagram of Ga-H formation on 4CN Ga site with dehydration (T = 250°C, PH2O = 10-9 atm) c) Free energy diagram of oligomerization on Ga-H (T = 250°C) d) Schematic of ethylene oligomerization on Ga-H and the associated reaction intermediates

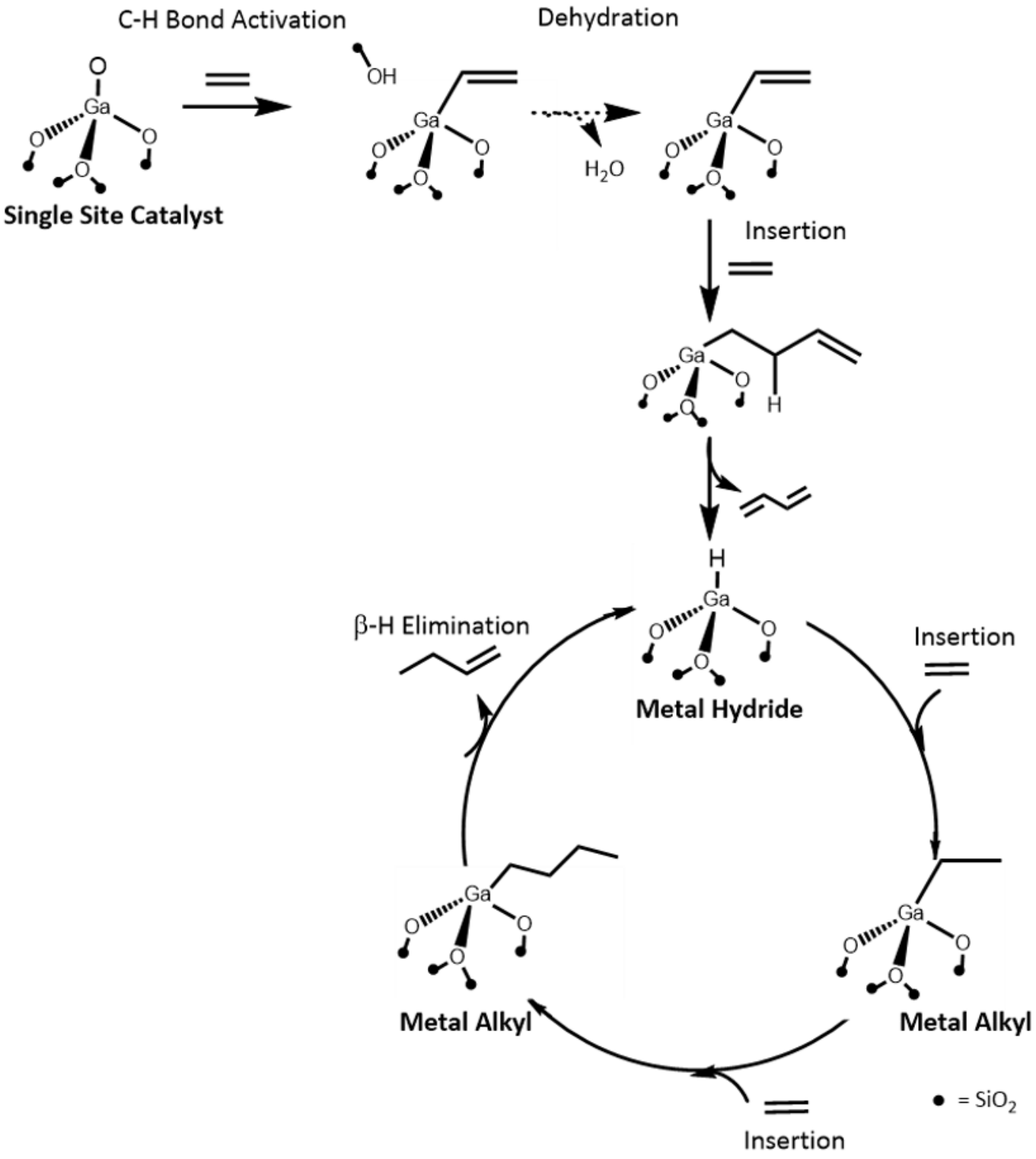


**Figure 4**

Proposed heterogeneous oligomerization reaction pathway for single site Ga3+ catalysts on silica

# Supplementary Files

This is a list of supplementary files associated with this preprint. Click to download.

- Scheme1.png
- NatureCommSI1020.docx